*Indian J Phys (July 2026) 100(8):3357–3368*
https://doi.org/10.1007/s12648-026-04021-8

ORIGINAL PAPER

# Traveling wave solutions for a normalized time-fractional predator–prey model

**S Ham[1], S Kwak[1], A Yun[2], Jyoti[3], Y Nam[4], H Kim[5] and J Kim[1]***

[1]Department of Mathematics, Korea University, Seoul 02841, Republic of Korea

[2]Liberal Arts and Science, Korea Aerospace University, Goyang-si, Gyeonggi-do, Republic of Korea

[3]The Institute of Basic Science, Korea University, Seoul 02841, Republic of Korea

[4]Program in Actuarial Science and Financial Engineering, Korea University, Seoul 02841, Republic of Korea

[5]Department of Mathematics and Physics, Gangneung-Wonju National University, Gangneung, Republic of Korea

Received: 30 October 2025 / Accepted: 11 March 2026 / Published online: 25 March 2026

**Abstract** We introduce a normalized time-fractional diffusive predator–prey model that accounts for memory effects through a novel fractional time scale. Unlike conventional time-fractional models, the proposed formulation uses a normalized fractional derivative that ensures the total weight of the memory kernel remains unity, which enables a more consistent interpretation of historical influence across all fractional orders. The model is discretized using a finite difference scheme and solved via tridiagonal systems. Numerical simulations are performed to study traveling wave solutions and the dynamics of the system under varying fractional orders. The computational results demonstrate that decreasing the order of the fractional derivative leads to shorter temporal periods and increased spatial wavelengths in the predator–prey oscillations, while simultaneously reducing the amplitude of population fluctuations. These numerical experiments highlight the important role of fractional order in controlling the temporal and spatial evolution of ecological systems and emphasize the advantages of normalization in analyzing such dynamics.

**Keywords:** Predator–prey system; Time-fractional derivative; Traveling wave solution; Finite difference method

## 1. Introduction

The Lotka–Volterra model, introduced by [1, 2] in the early 20th century, is a prominent mathematical tool used to describe the interactions between two species: the 'prey', which is hunted, and the 'predator', which hunts [3]. This model reveals how the population sizes of both species affect each other over time through their biological relationships. The model is also represented by nonlinear differential equations, which have been applied in numerous studies to study various biological and ecological cases [4], including interactions among susceptible and infectious populations, plant and herbivore relationships, virus and immune system interactions, parasite-host relationships, and resource-consumer dynamics [5]. He et al. [6] proposed an extreme learning machine technique to solve the Lotka–Volterra predator–prey system with discrete delays.

In this study, we focused on the diffusive nature of the model to handle the spatial heterogeneity of the environment that influences predator–prey interactions. In this respect, Swailem and Täuber [3] used a stochastic spatial Lotka–Volterra model subject to a periodically varying carrying capacity to investigate the dynamics of predator and prey by using Monte Carlo simulations. Furthermore, Arif et al. [7] used the Lyapunov method to find the stability of the diffusive and non-diffusive predator–prey systems with consuming resources in which prey is affected with some infectious disease. Ma et al. [8] applied Lyapunov–Schmidt reduction method to investigate the dynamical behavior of a diffusive Lotka–Volterra system incorporating fear effects, subject to the Neumann boundary conditions. In addition, to investigate the implications of population heterogeneity for population growth, Waters

*Corresponding author, E-mail: cfdkim@korea.ac.kr

et al. [9] developed logistic and competitive Lotka–Volterra equations by using the Eizi Kuno model.

However, to describe more complex biological or ecological systems which have memory effects [10, 11], anomalous diffusion [12], and non-local interactions [13], a simple integer order predator–prey model is not enough. For such situations we need a non-integer order or fractional-order predator–prey model [4, 5]. Alqhtani et al. [14] studied spatiotemporal pattern formation in sub-diffusive predator–prey system with the Caputo fractional derivative. El-Saka et al. [15] examined the effects of economic profit and fractional-order derivatives on the local stability of predator–prey system. In [16], the authors studied the dynamics of a fractional-order delay differential predator–prey model that incorporates multiple feedback time delays and a Holling-type III functional response. Kumar et al. [17] investigated complex dynamics behavior on time-fractional predator–prey model. Kashif and Singh [18] presented a numerical scheme for time-fractional advection–diffusion-reaction predator–prey model for variable fractional order. The existence and uniqueness of the solutions are proved with Ulam–Hyer stability. Das et al. [19] investigated three-dimensional fractional slow-fast prey-predator model. Additionally, it is important to describe the propagation of predators and prey across space, the spread of disturbances such as diseases or environmental changes, and the stability of a diffusive predator–prey system, where traveling waves play a crucial role [20, 21]. Recently, qualitative and analytical studies on traveling wave solutions have also been actively investigated in various nonlinear and stochastic partial differential equations. For instance, Wang and Li [22] analyzed the dynamics and traveling wave solutions of a stochastic nonlinear Kodama equation in the Stratonovich sense.

By considering all these factors, we explored the literature and found very few studies, which provided traveling wave solutions of the fractional-order predator–prey model. For example, Choi et al. [23] used the Q-function method to find the spread of two species by using fractional coupled reaction-diffusion differential equation and found the exact solution in the form of traveling wave. Areshi et al. [24] derived solitary wave solutions for a predator–prey model using fractional-order derivatives. The solutions were expressed using a variety of functions, including trigonometric, hyperbolic, exponential, and rational forms using Mathematica as the primary computational tool. Tang [25] used fractional-order Lotka–Volterra model to analyse the existence, uniqueness, and non-negativity of the system. By applying Laplace transform and Hopf bifurcation theory of fractional-order dynamical systems, they found sufficient criteria that guarantee local stability of the system. Nikolova [26] applied the Simple Equations Method to derive traveling wave solutions for two fractional-order partial differential equations that model predator–prey interactions, incorporating the Allee effect for both species. Moreover, Mansour [27] employed traveling wave methods to numerically analyze wavefront pattern formation in a fractional partial differential equation system influenced by anomalous subdiffusion. Through computer simulations, it was observed that traveling waves propagate more rapidly in sub-diffusive systems compared to their normal diffusive, time-dependent counterparts.

In addition to predator–prey systems, traveling wave theory for delayed reaction–diffusion models has been developed in epidemic-type methods. For instance, a reaction–diffusion addiction epidemic model with distributed delays shows an $R_0$-threshold phenomenon: when $R_0 > 1$, a minimal wave speed $c^* > 0$ exists and nontrivial traveling waves occur for $c \leq c^*$, whereas such waves do not exist when $R_0 < 1$ (or when $c < c^*$) [28]. Similar $R_0$-dependent existence and nonexistence results, together with minimal-speed characterizations, also appear in delayed reaction–diffusion SIR models with generalized incidence, both single-group settings and in heterogeneous multi-group extensions [29, 30]. From an ecological perspective, spatial predator–prey models that include herd behavior and nonlocal interactions can generate rich spatiotemporal dynamics, such as Turing and Turing–Hopf instabilities and pattern formation under Neumann boundary conditions. Moreover, fractional-order multi-species predator–prey methods that account for partial prey escape from a herd exhibit complex dynamical features, such as stability switching and bifurcation behavior, and the fractional order plays a decisive role in these phenomena [31, 32]. These developments motivate a broader view of time-fractional predator–prey traveling waves. The present study relates the proposed analysis to delayed and nonlocal reaction–diffusion wave studies and highlights ecological mechanisms, such as herd-mediated interactions, that can alter wave and pattern dynamics.

From the literature, we observed that using a time-fractional derivative in a predator–prey model poses challenges in examining the impact of the order parameter $\alpha$ by making direct comparisons at identical time points due to the lack of time normalization in the Caputo fractional derivative [33–35]. To resolve this factor in the present study, we adopted the normalized time-fractional derivative. We extend the work of [36, 37], which introduced a normalized time-fractional diffusion equation, by proposing a novel normalized time-fractional predator–prey model to study the effects of order parameter $\alpha$. We numerically examine the dynamics of species by using a finite difference method (FDM). The model incorporates a distinctive time scale that differs from traditional time-fractional approaches. This time scale clarifies the

fractional time derivative as a weighted average of the system's history, and it ensures the total weight remains unity for any fractional parameter or time [38]. This property allows for a precise analysis of how fractional order influences system behavior. Numerical tests show that the proposed equation outperforms conventional approaches and effectively captures complex dynamics.

The remaining part of the paper is organized as follows: Section 2 presents the mathematical equation, while in Sect. 3, computational scheme is developed to give numerical solution and in Sect. 4 numerical experiments are performed by using an algorithm and finally, the conclusion is provided in Sect. 5.

## 2. The governing system

For the non-negative population densities of prey and predator, denoted by $u(x, t)$ and $v(x, t)$ respectively, at position $x$ and time $t$, the governing system is given as follows:

$$\frac{\partial^\alpha u(x,t)}{\partial t^\alpha} = \Delta u(x,t) + u(x,t)(1-u(x,t)) - \frac{\gamma u(x,t)v(x,t)}{1+\gamma u(x,t)}, \tag{1}$$

$$\frac{\partial^\alpha v(x,t)}{\partial t^\alpha} = \sigma\Delta v(x,t) + \frac{\gamma u(x,t)v(x,t)}{\beta(1+\gamma u(x,t))} - \frac{v(x,t)}{a\beta}, \ x \in \Omega, \quad t > 0, \tag{2}$$

where $a$, $\beta$, $\gamma$, and $\sigma$ are positive dimensionless parameters. Here $\Omega = (L_x,\ R_x)$ is the domain and the normalized time-fractional derivative is defined as follows [36, 39, 40]:

$$\frac{\partial^\alpha f(x,t)}{\partial t^\alpha} = \frac{1-\alpha}{t^{1-\alpha}} \int_0^t \frac{\partial f(x,s)}{\partial s} \frac{ds}{(t-s)^\alpha}, \quad 0 < \alpha < 1, \tag{3}$$

where the factor $(1-\alpha)/t^{1-\alpha}$ is a normalization constant ensuring that

$$\frac{1-\alpha}{t^{1-\alpha}} \int_0^t \frac{ds}{(t-s)^\alpha} = 1. \tag{4}$$

From Eq. (4), we define the weight function $w_\alpha^t(s)$ as

$$w_\alpha^t(s) = \frac{1-\alpha}{t^{1-\alpha}(t-s)^\alpha},$$

which satisfies the normalization condition [41]:

$$\int_0^t w_\alpha^t(s)ds = 1.$$

The governing system (1)–(2) possesses equilibrium points at (0, 0), (1, 0) and $(\bar{u}, \bar{v})$, where $\bar{u}$ and $\bar{v}$ are specified as

$$\bar{u} = \frac{1}{\gamma(a-1)} \quad \text{and} \quad \bar{v} = \frac{(1-\bar{u})(1+\gamma\bar{u})}{\gamma}.$$

In order to ensure the positivity of $\bar{u}$ and $\bar{v}$, it is required that $a > 1$. The boundary conditions on $\partial\Omega$ are zero Dirichlet and Neumann boundary conditions at the left endpoint $x = L_x$ and right end point $x = R_x$, respectively:

$$u(L_x,t) = v(L_x,t) = 0 \text{ and } \frac{\partial u(R_x,t)}{\partial x} = \frac{\partial v(R_x,t)}{\partial x} = 0. \tag{5}$$

The homogeneous Dirichlet boundary condition implies that both the predator and prey populations are zero at the boundary, while the homogeneous Neumann boundary condition indicates that there is no flux across the boundary.

## 3. Numerical solutions

The computational domain $\Omega = (L_x, R_x)$ is discretized as follows: $\Omega_h = \{x_i | x_i = L_x + (i-1)h,\ 1 \le i \le N_x\}$, where $h = (R_x - L_x)/(N_x - 0.5)$, see Fig. 1.

We define $u_i^n = u(x_i, t_n)$, $v_i^n = v(x_i, t_n)$, and $t_n = (n-1)\Delta t$, where $\Delta t$ represents the time step. Equation (3) can be approximated using the following quadrature formula:

$$\frac{\partial^\alpha f(x_i,t_{n+1})}{\partial t^\alpha} = \frac{1-\alpha}{t_{n+1}^{1-\alpha}} \sum_{p=1}^{n} \int_{t_p}^{t_{p+1}} \frac{\partial f(x_i,s)}{\partial s} \frac{ds}{(t_{n+1}-s)^\alpha} \approx \sum_{p=1}^{n} \frac{1-\alpha}{t_{n+1}^{1-\alpha}} \int_{t_p}^{t_{p+1}} \frac{ds}{(t_{n+1}-s)^\alpha} \frac{f_i^{p+1} - f_i^p}{\Delta t} \tag{6}$$

$$= \sum_{p=1}^{n} \frac{(n+1-p)^{1-\alpha} - (n-p)^{1-\alpha}}{n^{1-\alpha}} \frac{f_i^{p+1} - f_i^p}{\Delta t}, \tag{7}$$

where $\partial f(x_i, s)/\partial s$ over an interval $[t_p,\ t_{p+1}]$ is approximated using the finite difference $(f_i^{p+1} - f_i^p)/\Delta t$ in Eq. (6). As a result, we derive the following FDM using the formula (7):

$$\sum_{p=1}^{n} w_p^n \frac{u_i^{p+1} - u_i^p}{\Delta t} = \frac{u_{i-1}^{n+1} - 2u_i^{n+1} + u_{i+1}^{n+1}}{h^2} + F_i^n, \tag{8}$$

$$\sum_{p=1}^{n} w_p^n \frac{v_i^{p+1} - v_i^p}{\Delta t} = \sigma \frac{v_{i-1}^{n+1} - 2v_i^{n+1} + v_{i+1}^{n+1}}{h^2} + G_i^n, \tag{9}$$

where $w_p^n = [(n+1-p)^{1-\alpha} - (n-p)^{1-\alpha}]/n^{1-\alpha}$ is a discrete weight parameter,

**Fig. 1** Discrete domain

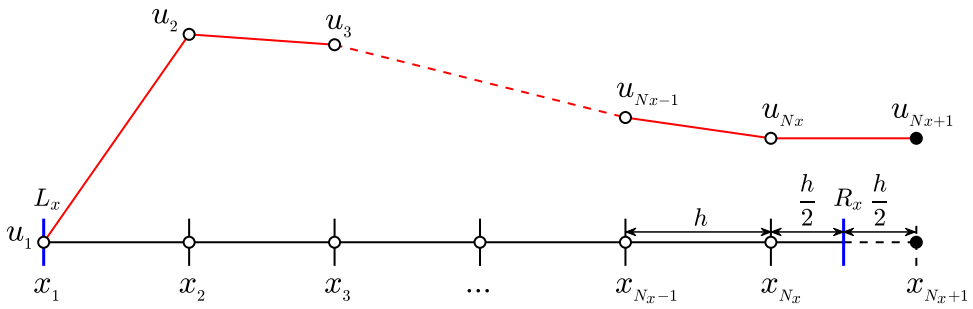


$$F_i^n = u_i^n(1-u_i^n) - \frac{\gamma u_i^n v_i^n}{1+\gamma u_i^n}, \text{ and } G_i^n = \frac{\gamma u_i^n v_i^n}{\beta(1+\gamma u_i^n)} - \frac{v_i^n}{a\beta}. \tag{10}$$

For any value of $n$, the weight parameter $w_p^n$ satisfies the following relation: $\sum_{p=1}^{n} w_p^n = 1$. Equations (8) and (9) can then be reformulated as follows:

$$\begin{aligned} &-\frac{1}{h^2}u_{i-1}^{n+1} + \left(\frac{w_n^n}{\Delta t} + \frac{2}{h^2}\right)u_i^{n+1} - \frac{1}{h^2}u_{i+1}^{n+1} \\ &= \frac{w_n^n}{\Delta t}u_i^n + F_i^n - \sum_{p=1}^{n-1} w_p^n \frac{u_i^{p+1} - u_i^p}{\Delta t}, \end{aligned} \tag{11}$$

$$\begin{aligned} &-\frac{\sigma}{h^2}v_{i-1}^{n+1} + \left(\frac{w_n^n}{\Delta t} + \frac{2\sigma}{h^2}\right)v_i^{n+1} - \frac{\sigma}{h^2}v_{i+1}^{n+1} \\ &= \frac{w_n^n}{\Delta t}v_i^n + G_i^n - \sum_{p=1}^{n-1} w_p^n \frac{v_i^{p+1} - v_i^p}{\Delta t}. \end{aligned} \tag{12}$$

Equations (11) and (12) are tridiagonal systems with zero Dirichlet and Neumann boundary conditions and the Thomas algorithm [42] can be employed to obtain the solution of this system efficiently [43]. Consequently, the vector $\mathbf{u}^{n+1}$ for the numerical solutions is obtained by solving the following tridiagonal system:

$$A\mathbf{u}^{n+1} = \mathbf{f},$$

where $A$ is a tridiagonal matrix imposing zero Dirichlet boundary conditions at $x = L_x$ ($u_1^{n+1} = 0$) and zero Neumann boundary conditions at $x = R_x$ ($u_{N_x+1}^{n+1} = u_{N_x}^{n+1}$):

$$A = \begin{pmatrix} \frac{w_n^n}{\Delta t} + \frac{2}{h^2} & -\frac{1}{h^2} & 0 & \cdots & 0 & 0 & 0 \\ -\frac{1}{h^2} & \frac{w_n^n}{\Delta t} + \frac{2}{h^2} & -\frac{1}{h^2} & \cdots & 0 & 0 & 0 \\ 0 & -\frac{1}{h^2} & \frac{w_n^n}{\Delta t} + \frac{2}{h^2} & \cdots & 0 & 0 & 0 \\ \vdots & \vdots & \vdots & \ddots & \vdots & \vdots & \vdots \\ 0 & 0 & 0 & \cdots & -\frac{1}{h^2} & \frac{w_n^n}{\Delta t} + \frac{2}{h^2} & -\frac{1}{h^2} \\ 0 & 0 & 0 & \cdots & 0 & -\frac{1}{h^2} & \frac{w_n^n}{\Delta t} + \frac{1}{h^2} \end{pmatrix},$$

$$\mathbf{u}^{n+1} = \begin{pmatrix} u_2^{n+1} \\ u_3^{n+1} \\ \vdots \\ u_{N_x}^{n+1} \end{pmatrix}, \text{ and } \mathbf{f} = \begin{pmatrix} w_n^n u_2^n/\Delta t - F_2^n \\ w_n^n u_3^n/\Delta t - F_3^n \\ \vdots \\ w_n^n u_{N_x}^n/\Delta t - F_{N_x}^n \end{pmatrix}.$$

Here, $F_i^n = \sum_{p=1}^{n-1} w_p^n (u_i^{p+1} - u_i^p)/\Delta t$. Similarly, we solve the tridiagonal system $B\mathbf{v}^{n+1} = \mathbf{g}$, where $B$ is a tridiagonal matrix imposing zero Dirichlet at $x = L_x$ ($v_1^{n+1} = 0$) and zero Neumann boundary condition at $x = R_x$ ($v_{N_x+1}^{n+1} = v_{N_x}^{n+1}$)

$$B = \begin{pmatrix} \frac{w_n^n}{\Delta t} + \frac{2\sigma}{h^2} & -\frac{\sigma}{h^2} & 0 & \cdots & 0 & 0 & 0 \\ -\frac{\sigma}{h^2} & \frac{w_n^n}{\Delta t} + \frac{2\sigma}{h^2} & -\frac{\sigma}{h^2} & \cdots & 0 & 0 & 0 \\ 0 & -\frac{\sigma}{h^2} & \frac{w_n^n}{\Delta t} + \frac{2\sigma}{h^2} & \cdots & 0 & 0 & 0 \\ \vdots & \vdots & \vdots & \ddots & \vdots & \vdots & \vdots \\ 0 & 0 & 0 & \cdots & -\frac{\sigma}{h^2} & \frac{w_n^n}{\Delta t} + \frac{2\sigma}{h^2} & -\frac{\sigma}{h^2} \\ 0 & 0 & 0 & \cdots & 0 & -\frac{\sigma}{h^2} & \frac{w_n^n}{\Delta t} + \frac{\sigma}{h^2} \end{pmatrix},$$

$$\mathbf{v}^{n+1} = \begin{pmatrix} v_2^{n+1} \\ v_3^{n+1} \\ \vdots \\ v_{N_x}^{n+1} \end{pmatrix}, \text{ and } \mathbf{g} = \begin{pmatrix} w_n^n v_2^n/\Delta t - G_2^n \\ w_n^n v_3^n/\Delta t - G_3^n \\ \vdots \\ w_n^n v_{N_x}^n/\Delta t - G_{N_x}^n \end{pmatrix}.$$

Here, $G_i^n = \sum_{p=1}^{n-1} w_p^n (v_i^{p+1} - v_i^p)/\Delta t$. This numerical algorithm provides an efficient method for computing time-fractional predator–prey dynamics and offers a consistent approach that accounts for the temporal memory effects inherent in the model. For future work, we will adopt a high-order stable numerical scheme to further improve the numerical stability and to use larger time step sizes [44].

## 4. Numerical experiments

We study the effect of the normalized fractional time derivative on the traveling wave solutions of the one-dimensional predator–prey model. In the following numerical experiments, we use the following fixed nondimensionalized parameters $a = 1.8$, $\beta = 1.2$, $\gamma = 4.9$, and $\sigma = 2.5$.

### 4.1. Kinetic system

A traveling wave solution can exist when the kinetic system without diffusion terms exhibits a stable limit cycle. To investigate the existence of the traveling wave solution of the predator–prey model, we examine the following kinetic system:

$$\frac{\partial^\alpha u(t)}{\partial t^\alpha} = f(u,v) = u(t)(1-u(t)) - \frac{\gamma u(t) v(t)}{1+\gamma u(t)}, \tag{13}$$

$$\frac{\partial^\alpha v(t)}{\partial t^\alpha} = g(u,v) = \frac{\gamma u(t) v(t)}{\beta(1+\gamma u(t))} - \frac{v(t)}{a\beta}. \tag{14}$$

To analyze the stability of the equilibrium points: (0, 0), (1, 0), and $(\bar{u}, \bar{v})$, we linearize the kinetic system (13)–(14) using the following Jacobian matrix [45]

$$J(u,v) = \begin{pmatrix} f_u(u,v) & f_v(u,v) \\ g_u(u,v) & g_v(u,v) \end{pmatrix},$$

with

$$f_u(u,v) = 1 - 2u - \frac{\gamma v}{1+\gamma u} + \frac{\gamma^2 uv}{(1+\gamma u)^2},$$

$$f_v(u,v) = -\frac{\gamma u}{1+\gamma u},$$

$$g_u(u,v) = \frac{\gamma v}{\beta(1+\gamma u)^2},$$

$$g_v(u,v) = \frac{\gamma u}{\beta(1+\gamma u)} - \frac{1}{a\beta}.$$

The eigenvalues of the Jacobian matrix $J$ are roots of the characteristic polynomial

$$\det(\lambda I - J) = \lambda^2 - (\operatorname{tr} J)\lambda + \det J,$$

where $\det J$ and $\operatorname{tr} J$ are the determinant and the trace of the Jacobian matrix $J$, respectively. Hence,

$$\lambda_{1,2} = \frac{\operatorname{tr} J \pm \sqrt{(\operatorname{tr} J)^2 - 4\det J}}{2}.$$

For the equilibrium point (0, 0), the Jacobian matrix is given by

$$J(0,0) = \begin{pmatrix} 1 & 0 \\ 0 & -\frac{1}{a\beta} \end{pmatrix}.$$

The corresponding eigenvalues are $\lambda_1 = 1$ and $\lambda_2 = -1/(a\beta)$. Since one eigenvalue is positive and the other is negative, the equilibrium point (0, 0) is a saddle point and hence unstable. For the equilibrium point (1, 0), the Jacobian matrix is

$$J(1,0) = \begin{pmatrix} -1 & -\frac{\gamma}{1+\gamma} \\ 0 & \frac{\gamma}{\beta(1+\gamma)} - \frac{1}{a\beta} \end{pmatrix}.$$

The eigenvalues of the matrix are

$$\lambda_1 = -1 \quad \text{and} \quad \lambda_2 = \frac{\gamma}{\beta(1+\gamma)} - \frac{1}{a\beta}.$$

Therefore, the stability depends on the sign of $\lambda_2$. If $\frac{\gamma}{1+\gamma} > \frac{1}{a}$, then $\lambda_2 > 0$ and (1, 0) is a saddle point; otherwise, it is locally asymptotically stable. Finally, for the equilibrium point $(\bar{u}, \bar{v})$, the Jacobian matrix is given by

$$J(\bar{u},\bar{v}) = \begin{pmatrix} \frac{1}{a} - \frac{a+1}{a\gamma(a-1)} & -\frac{1}{a} \\ \frac{\gamma(a-1)-1}{a\beta\gamma} & 0 \end{pmatrix},$$

the determinant of the Jacobian matrix at $(\bar{u},\bar{v})$ is given by

$$\det J(\bar{u},\bar{v}) = \frac{\gamma(a-1)-1}{a^2\beta\gamma}.$$

Hence, for $a > 1$ and $\beta > 0$, we have $\det J(\bar{u},\bar{v}) > 0$. In particular, if

$$(\mathrm{tr}\ , J(\bar{u},\bar{v}))^2 - 4\det J(\bar{u},\bar{v}) < 0,$$

then the eigenvalues form a complex conjugate pair and $(\bar{u},\bar{v})$ is a focus. Moreover, a Hopf bifurcation occurs when $\mathrm{tr}\ J(\bar{u},\bar{v}) = 0$. The system undergoes Hopf bifurcation at

$$\mathrm{tr}\ J(\bar{u},\bar{v}) = \frac{1}{a} - \frac{a+1}{a\gamma(a-1)} = 0 \quad \Longleftrightarrow \quad \gamma = \frac{a+1}{a-1}.$$

Therefore, when $\gamma$ crosses the critical value $\gamma_H = \frac{a+1}{a-1}$ $(a > 1)$, the equilibrium point $(\bar{u},\bar{v})$ changes stability through a Hopf bifurcation.

The kinetic system given by Eqs. (13) and (14) is discretized as follows:

$$\sum_{p=1}^{n} w_p^n \frac{u^{p+1} - u^p}{\Delta t} = F^n, \tag{15}$$

$$\sum_{p=1}^{n} w_p^n \frac{v^{p+1} - v^p}{\Delta t} = G^n, \tag{16}$$

where $u^n = u(n\Delta t)$, $v^n = v(n\Delta t)$,

$$F^n = u^n(1-u^n) - \frac{\gamma u^n v^n}{1+\gamma u^n}, \quad \text{and} \quad G^n = \frac{\gamma u^n v^n}{\beta(1+\gamma u^n)} - \frac{v^n}{a\beta}.$$

By using Eqs. (15) and (16), the numerical solution can be explicitly obtained as

$$u^{n+1} = u^n + \frac{\Delta t}{w_n^n}\left(F^n - \sum_{p=1}^{n-1} w_p^n \frac{u^{p+1} - u^p}{\Delta t}\right),$$

$$v^{n+1} = v^n + \frac{\Delta t}{w_n^n}\left(G^n - \sum_{p=1}^{n-1} w_p^n \frac{v^{p+1} - v^p}{\Delta t}\right).$$

Based on the linear stability analysis, when the parameter $\gamma$ crosses $\gamma_H$, the equilibrium point $(\bar{u},\bar{v})$ loses stability through a Hopf bifurcation, leading to the emergence of periodic oscillations. To illustrate this bifurcation structure, we consider two representative cases: $\gamma < \gamma_H$ and $\gamma > \gamma_H$. For the given parameter $a = 1.9$, Fig. 2(a) shows $\mathrm{tr}\ J(\bar{u},\bar{v})$ for $\gamma$. Figure 2 illustrates the phase portraits of the predator–prey system for different fractional orders $\alpha = 0.96$, 0.98, and 1. Here, the initial condition is given as $(u(0), v(0)) = (\bar{u} - 0.05, \bar{v})$. When $\gamma = 3 < \gamma_H$, the equilibrium point remains stable, and the trajectories spiral toward $(\bar{u},\bar{v})$ for all tested values of $\alpha$. In contrast, for $\gamma = 4 > \gamma_H$, a stable limit cycle emerges, which confirms the occurrence of a Hopf bifurcation. As the fractional order $\alpha$ decreases, noticeable changes appear in the size and shape of the limit cycles, which indicates that the fractional-order dynamics modulate the amplitude and spatial extent of the oscillations and preserve the qualitative bifurcation structure.

Figure 3 illustrates the phase portraits originating from two distinct initial points, $(u,v) = (\bar{u} - 0.05, \bar{v})$ and $(u,v) = (\bar{u} + 0.65, \bar{v})$, governed by different fractional orders $\alpha = 1$, $\alpha = 0.98$, $\alpha = 0.96$, $\alpha = 0.94$. The red square markers denote the equilibrium point $(\bar{u},\bar{v})$ and the blue solid line in each subfigure represents the stable limit cycle, which demonstrates the periodic behavior toward which trajectories converge over time. Figure 4 shows superimposed limit cycles from Fig. 3 with the directional field for four different fractional orders: $\alpha = 1$, $\alpha = 0.98$, $\alpha = 0.96$, and $\alpha = 0.94$. The computational results shown in Figs. 3 and 4 highlight the effect of the fractional order $\alpha$ on the shape and size of the limit cycle and show that, as $\alpha$ decreases, the limit cycle becomes smaller and shifts closer to $(\bar{u},\bar{v})$, which indicates changes in the system dynamics. Figure 5 illustrates the temporal evolution of the state variables $u(t)$ and $v(t)$ in the ordinary kinetic system for fractional orders $\alpha = 1$, 0.98, 0.96, and 0.94. Here, $\Delta t = 0.02$, and the initial values are set as $u(0) = \bar{u} - 0.05$ and $v(0) = \bar{v}$ for the computational tests. In all cases, the system exhibits periodic behavior, but the period and amplitude of the oscillations are influenced by the fractional order. The results in Fig. 5 demonstrate the oscillations of the system become progressively faster, with shorter periods and reduced amplitudes. This suggests that as the fractional order $\alpha$ decreases, the period of the solution in the predator–prey model is expected to shorten. To quantitatively characterize the key phenomena shown in Fig. 5, we investigate the period and amplitude of the numerical solutions using the following definitions. The initial transient regime is excluded by restricting the analysis to the time interval $t \geq t_{\mathrm{trans}}$, where a fixed time $t_{\mathrm{trans}} = 40$ is used. Let $w(t)$ denote the numerical solution in a transient regime $t \geq t_{\mathrm{trans}}$. We detect the local maxima of $w(t)$ in this regime and denote the times of the first two successive local maxima by $t_1$ and $t_2$. The numerical period is defined as the time difference between these two successive maximum as

$$'P_w := t_2 - t_1.$$

For the same transient regime $t \geq t_{\mathrm{trans}}$, the numerical amplitude of $w(t)$ is defined as

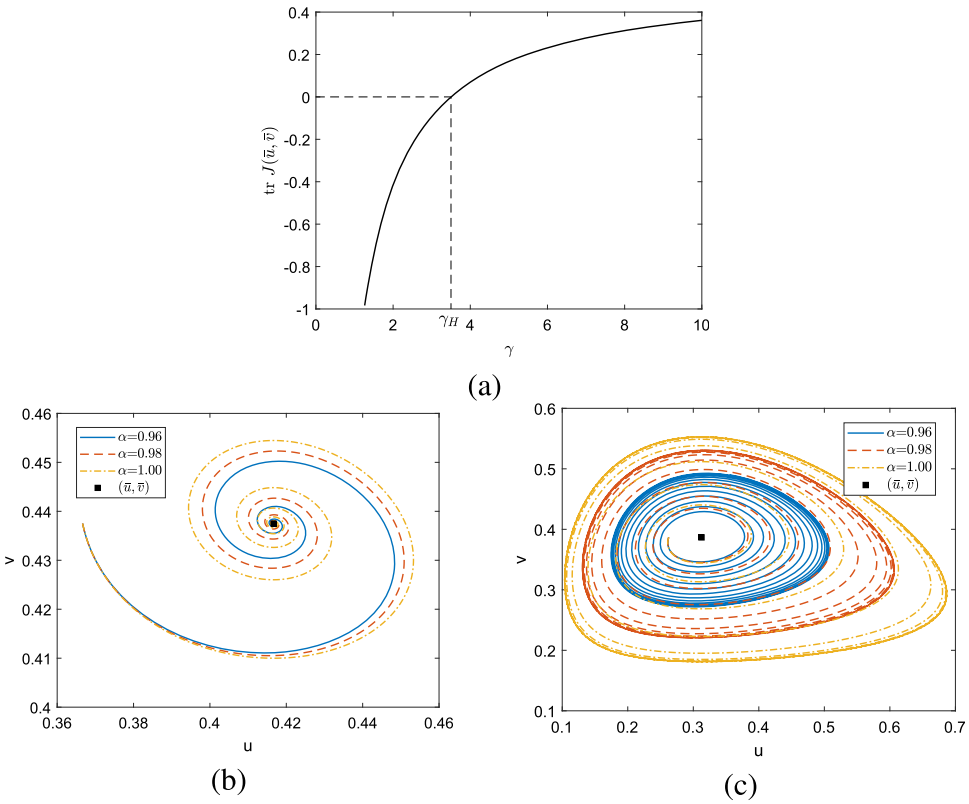


**Fig. 2** (**a**) Trace of the Jacobian matrix $\mathrm{tr}\, J(\bar{u},\bar{v})$ as a function of $\gamma$, showing the critical value $\gamma_H$ at which a Hopf bifurcation occurs. (b)–(c) Phase portraits for $\gamma = 3$ and $\gamma = 4$, respectively for different fractional orders $\alpha$

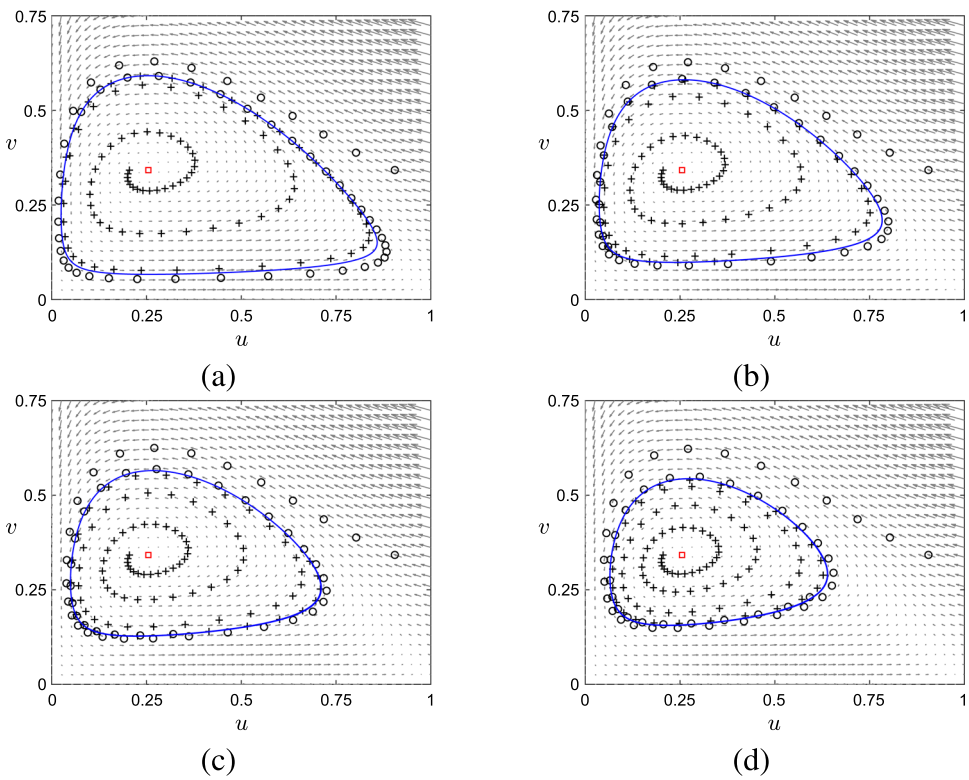


**Fig. 3** Phase portraits originating from two distinct initial points, $(u,v) = (\bar{u} - 0.05, \bar{v})$ and $(u,v) = (\bar{u} + 0.65, \bar{v})$ shown for directional fields with four different fractional orders: (**a**) $\alpha = 1$, (**b**) $\alpha = 0.98$, (**c**) $\alpha = 0.96$, and (**d**) $\alpha = 0.94$. Here, the red square marker denotes $(\bar{u},\bar{v})$, and the blue solid line indicates the stable limit cycle

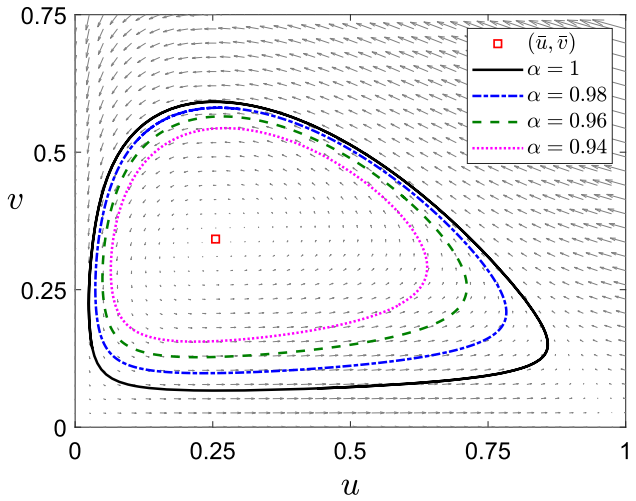


**Fig. 4** Superimposed limit cycles with the directional field for four different fractional orders: $\alpha = 1$, $\alpha = 0.98$, $\alpha = 0.96$, and $\alpha = 0.94$. Here, the red square marker represents the equilibrium point $(\bar{u}, \bar{v})$

$$A_w := w_{\max} - w_{\min},$$

where $w_{\max} = \max_{t \geq t_{\text{trans}}} w(t)$ and $w_{\min} = \min_{t \geq t_{\text{trans}}} w(t)$. Using these definitions, the numerical periods and amplitudes of $u(t)$ and $v(t)$ for different fractional orders $\alpha$ are summarized in Table 1. Table 1 shows that the fractional order $\alpha$ has a clear influence on the dynamics of the kinetic system. As $\alpha$ decreases, the numerical period of the oscillations decreases monotonically for both $u(t)$ and $v(t)$,

**Table 1** Numerical periods and amplitudes of $u$ and $v$ for various fractional orders $\alpha$ obtained from the kinetic system shown in Fig. 5

| $\alpha$ | $P_u$ | $P_v$ | $A_u$ | $A_v$ |
|---|---|---|---|---|
| 1.00 | 21.90 | 22.42 | 0.83 | 0.52 |
| 0.98 | 18.42 | 18.86 | 0.75 | 0.48 |
| 0.96 | 16.24 | 16.36 | 0.67 | 0.44 |
| 0.94 | 14.26 | 14.42 | 0.58 | 0.39 |

which indicates a shortening of the oscillation cycle. At the same time, the oscillation amplitudes $A_u$ and $A_v$ also decrease with decreasing $\alpha$, and this result reflects a progressive suppression of the magnitude of the cycle.

#### 4.1.1. *Comparison with the classical Caputo fractional order model*

We present a direct numerical comparison between the proposed normalized time-fractional model and the classical Caputo time-fractional model to clarify the practical impact of normalization. For comparison, the classical Caputo time-fractional kinetic system is given by

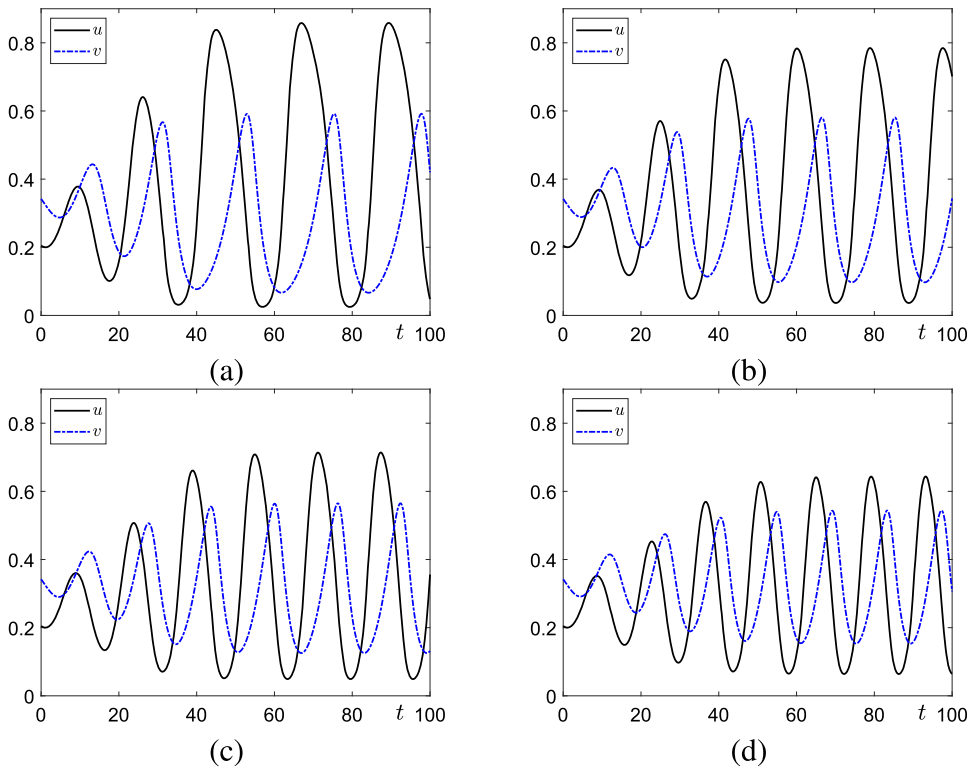


**Fig. 5** Temporal evolution of $u(t)$ and $v(t)$ for the ordinary differential kinetic system under different fractional orders: (**a**) $\alpha = 1$, (**b**) $\alpha = 0.98$, (**c**) $\alpha = 0.96$, and (**d**) $\alpha = 0.94$

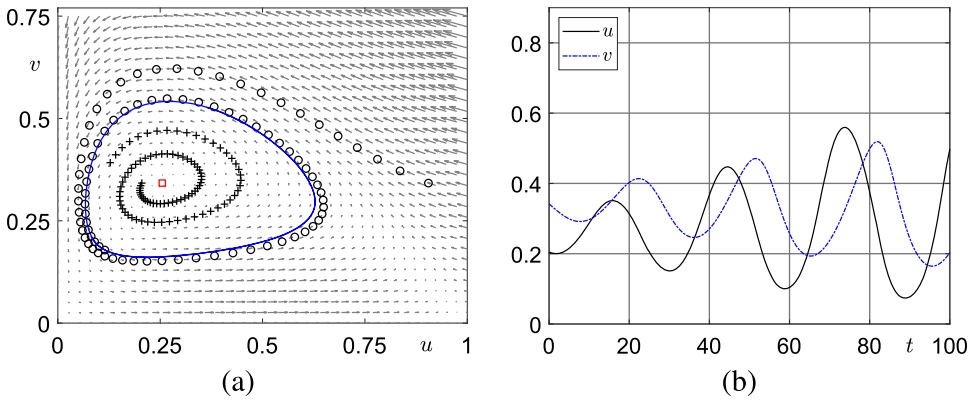


**Fig. 6** Numerical results obtained using the classical Caputo time-fractional derivative with $\bar{\alpha} = 0.94$. (**a**) Phase portrait of the kinetic system. (**b**) Temporal evolution of $u(t)$ and $v(t)$

$$\frac{\partial^{\bar{\alpha}} u(t)}{\partial t^{\bar{\alpha}}} = u(t)(1-u(t)) - \frac{\gamma u(t) v(t)}{1+\gamma u(t)},$$
$$\frac{\partial^{\bar{\alpha}} v(t)}{\partial t^{\bar{\alpha}}} = \frac{\gamma u(t) v(t)}{\beta(1+\gamma u(t))} - \frac{v(t)}{a\beta},$$

where $\partial^{\bar{\alpha}}/\partial t^{\bar{\alpha}}$ denotes the Caputo time-fractional derivative of order $\bar{\alpha} \in (0,1)$. The numerical experiment is performed for the fractional order $\bar{\alpha} = 0.94$, using the same initial conditions, time step size, and kinetic parameters as those adopted for the normalized formulation in Sect. 4.1.

Figure 6(a) shows the phase portrait obtained from the Caputo time-fractional system. Compared with the normalized result shown in Fig. 3(d), the Caputo-based trajectory exhibits a visibly distorted limit cycle and a slower convergence toward the periodic orbit. This indicates that the phase-space structure is more sensitive to the accumulated memory effect in the Caputo formulation. The corresponding temporal evolution of $u(t)$ and $v(t)$ computed using the Caputo derivative is shown in Fig. 6(b). Although oscillatory behavior persists, the Caputo-based solution shows a delayed convergence to the periodic orbit in the long-time regime when compared with the normalized result in Fig. 5(d). In contrast, the normalized time-fractional model approaches the periodic state more efficiently and exhibits a stable periodic behavior over the same time interval.

These results confirm that the normalized time-fractional model reduces excessive memory accumulation and provides a more efficient and robust description of long-time oscillatory behavior in the time-fractional predator–prey system.

### 4.2. Reaction-diffusion system

Next, we study the periodic traveling wave solution of the governing system (1)–(2). Figure 7 illustrates the spatiotemporal evolution of the periodic traveling wave solution for the prey and predator populations, denoted by $u$ and $v$, respectively, for the one-dimensional predator–prey model with different fractional orders: $\alpha = 1$, $\alpha = 0.98$, $\alpha = 0.96$, and $\alpha = 0.94$. We note that (a) $\alpha = 1$ corresponds to the classical system, while (b) $\alpha = 0.98$, (c) $\alpha = 0.96$, and (d) $\alpha = 0.94$ represent fractional-order dynamics. Here, the period of the solution is defined as the time interval between a given solution at a specific time at $t = T_0$ and the closest subsequent time at which the solution matches again during its evolution. The initial values are set as $u(x,0) = 2\bar{u}$ and $v(x,0) = 2\bar{v}$. The numerical parameters used are $N_x = 150$ and $\Delta t = 0.05h^2/\sigma$.

To quantitatively characterize the spatial wavelength and amplitude of the traveling wave solutions shown in Fig. 7, we introduce the following definitions. At a reference time $t = T_0$, the spatial wavelengths $\lambda_u$ and $\lambda_v$ for $u$ and $v$ are defined as the peak-to-peak spacing of the solution profile over the spatial domain. These spacings are illustrated by the blue line in Fig. 7(a)–(c). The amplitudes for $u$ and $v$ are defined as the spatial peak-to-peak values,

$$A_u := \max_x u(x, T_0) - \min_x u(x, T_0),$$
$$A_v := \max_x v(x, T_0) - \min_x v(x, T_0).$$

Table 2 lists the numerical spatial periods and amplitudes of $u(t)$ and $v(t)$ for different fractional orders $\alpha$ obtained from the numerical solutions shown in Fig. 7.

Compared with the classical derivative, it can be observed that as the fractional order $\alpha$ decreases, the temporal period of the traveling wave solution becomes shorter. This result is consistent with the expected behavior derived from the kinetic system solution. On the other hand, from a spatial perspective, examining the solution profiles reveals that as $\alpha$ decreases, the wavelength increases while the amplitude decreases. This indicates that the fractional order not only affects the temporal period but also the spatial structure of the solutions.

To examine the robustness of the fractional order effect with respect to parameter variations, we conduct a parameter test focusing on the predation rate parameter $\gamma$. From the bifurcation analysis in Sect. 4.1, the kinetic

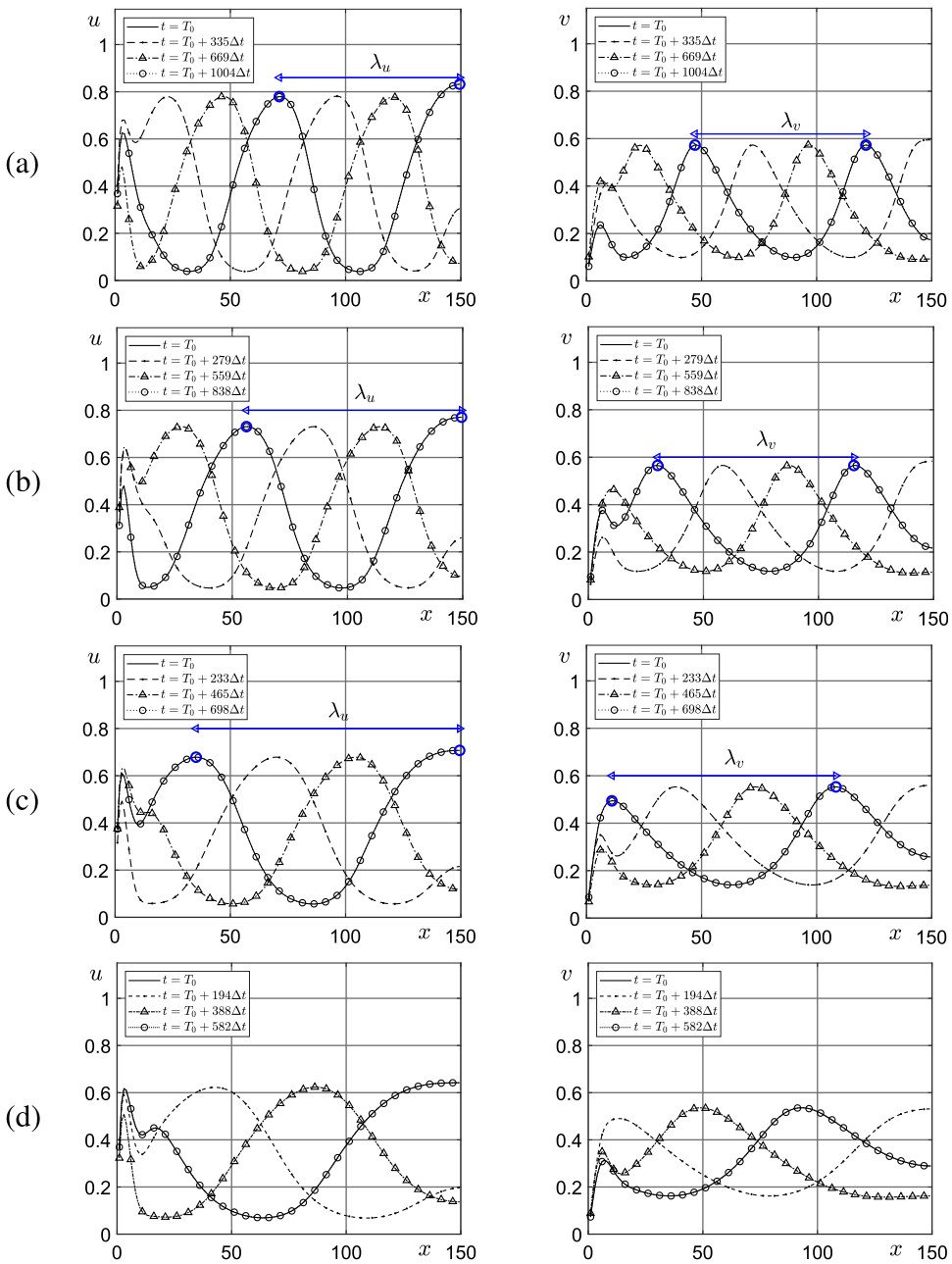


**Fig. 7** Periodic traveling wave solutions of the one-dimensional predator–prey model for different values of the fractional orders: (**a**) $\alpha = 1$, (**b**) $\alpha = 0.98$, (**c**) $\alpha = 0.96$, and (**d**) $\alpha = 0.94$. The left and right columns represent $u$ and $v$, respectively. Here, the parameters are fixed as $a = 1.8$, $\beta = 1.2$, $\gamma = 4.9$, and $\sigma = 2.5$

**Table 2** Numerical spatial periods and amplitudes of $u$ and $v$ for various fractional orders $\alpha$ obtained from the kinetic system shown in Fig. 7

| $\alpha$ | $\lambda_u$ | $\lambda_v$ | $A_u$ | $A_v$ |
|---|---|---|---|---|
| 1.00 | 78.26 | 74.25 | 0.79 | 0.51 |
| 0.98 | 93.31 | 85.28 | 0.72 | 0.47 |
| 0.96 | 114.38 | 97.32 | 0.65 | 0.47 |

system has a Hopf bifurcation at the critical value $\gamma_H = (a+1)/(a-1)$, where a stable limit cycle exists. This bifurcation structure provides a theoretical foundation for the existence of periodic traveling wave solutions in the reaction-diffusion system. Based on this analysis, we consider an alternative parameter setting with $\gamma = 4$, while keeping the remaining parameters fixed as $\alpha = 1.8$, $\beta = 1.2$, and $\sigma = 2.5$. Since $\gamma = 4 > \gamma_H$, the kinetic system still admits a limit cycle. Figure 8 shows the corresponding traveling wave solutions for different fractional orders. The numerical results in Fig. 8 demonstrate that, even with a reduced value $\gamma$, the influence of the fractional order remains unchanged: decreasing $\alpha$ consistently leads to a shortening of the temporal period of the traveling waves, accompanied by an increase in spatial wavelength and a

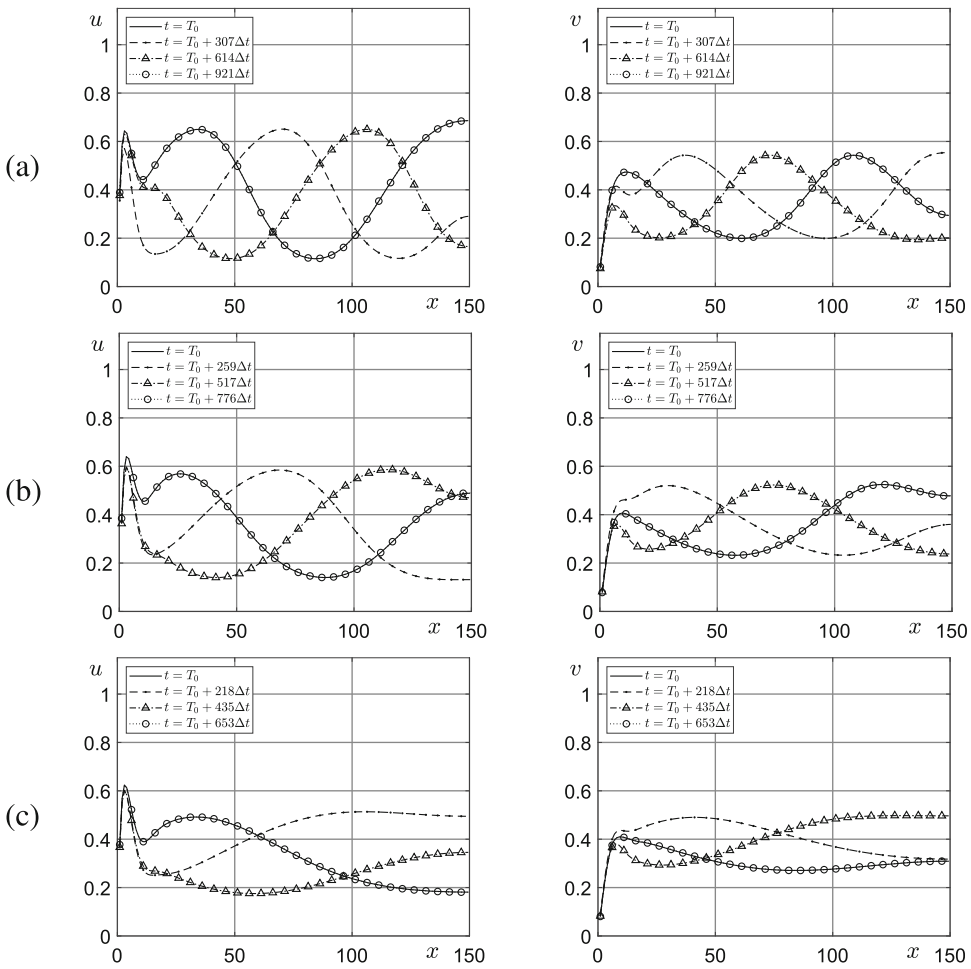


**Fig. 8** Periodic traveling wave solutions of the one-dimensional predator–prey model for different values of the fractional orders: (**a**) $\alpha = 1$, (**b**) $\alpha = 0.98$ and (**c**) $\alpha = 0.96$. The left and right columns represent $u$ and $v$, respectively. Here, the parameters are fixed as $a = 1.8$, $\beta = 1.2$, $\gamma = 4$, and $\sigma = 2.5$

reduction in amplitude. This indicates that a decrease in the fractional order $\alpha$ results in a shorter period, and that this behavior is preserved for different values of $\gamma$ within the parameter regime where a stable limit cycle exists.

## 5. Conclusions

We proposed the normalized time-fractional diffusive predator–prey system and conducted numerical investigations of its dynamics. Compared to the conventional time-fractional model, the proposed model ensures that the sum of the weights remains unity for all fractional parameters, and provides a more consistent interpretation of subdiffusion effects in predator–prey interactions. The proposed model is discretized and solved by using the FDM. Through numerical experiments, we analyzed the differences in performance between the normalized and conventional time-fractional predator–prey models. The results without diffusion demonstrated that as the fractional order $\alpha$ decreases, the period of oscillations shortens, while the amplitude of population fluctuations decreases. Additionally, we observed that the spatial structure of traveling wave solutions is significantly affected by the fractional order, with increasing wavelengths and diminishing amplitudes as $\alpha$ decreases. These findings indicate that fractional order plays a crucial role in shaping the temporal and spatial evolution of predator–prey interactions.

**Acknowledgements** The corresponding author (J.S. Kim) was supported by Korea University Grant. Hyundong Kim was supported by Basic Science Research Program through the National Research Foundation of Korea (NRF) funded by the Ministry of Education (RS-2025-25415913).

## References

[1] A J Lotka *Elements of Physical Biology* (Philadelphia: Williams & Wilkins) (1925)
[2] V Volterra *Nature* **119** 12 (1927). https://doi.org/10.1038/119012b0
[3] M S Swailem and U C Täuber *Phys. Rev. E* **107** 064144 (2023). https://doi.org/10.1103/PhysRevE.107.064144

[4] S Narayanamoorthy, D Baleanu, K Thangapandi and S S N Perera *IET Syst. Biol.* **13** 277 (2019). https://doi.org/10.1049/iet-syb.2019.0055
[5] P Panja *Int. J. Model. Simul.* **39** 256 (2019). https://doi.org/10.1080/02286203.2019.1611311
[6] J He, Z Zheng and Z Ye *Phys. A* **635** 129524 (2024). https://doi.org/10.1016/j.physa.2024.129524
[7] M S Arif, K Abodayeh and A Ejaz *Math. Biosci. Eng.* **20** 5066 (2023). https://doi.org/10.3934/mbe.2023235
[8] L Ma, H Wang and D Li *Z. Angew. Math. Phys.* **74** 106 (2023). https://doi.org/10.1007/s00033-023-01998-8
[9] E K Waters, H S Sidhu, L A Sidhu and G N Mercer *Ecol. Model.* **297** 187 (2015). https://doi.org/10.1016/j.ecolmodel.2014.11.019
[10] H L Li, L Zhang, C Hu, Y L Jiang and Z Teng *J. Appl. Math. Comput.* **54** 435 (2017). https://doi.org/10.1007/s12190-016-1017-8
[11] H L Li, A Muhammadhaji, L Zhang and Z Teng *Adv. Differ. Equ.* **2018** 325 (2018). https://doi.org/10.1186/s13662-018-1776-7
[12] Y Xie, J Lu and Z Wang *Phys. A* **526** 120773 (2019). https://doi.org/10.1016/j.physa.2019.04.009
[13] C Maji *Model. Earth Syst. Environ.* **8** 47 (2022). https://doi.org/10.1007/s40808-020-01061-9
[14] M Alqhtani, K M Owolabi and K M Saad *Chaos Solitons Fract.* **160** 112267 (2022). https://doi.org/10.1016/j.chaos.2022.112267
[15] H A A El-Saka, S Lee and B Jang *Nonlinear Dyn.* **96** 407 (2019). https://doi.org/10.1007/s11071-019-04796-y
[16] F A Rihan and C Rajivganthi *Chaos Solitons Fract.* **141** 110365 (2020). https://doi.org/10.1016/j.chaos.2020.110365
[17] A Kumar, D Bahuguna and S Kumar *J. Appl. Math. Comput.* **70** 5319 (2024). https://doi.org/10.1007/s12190-024-02171-8
[18] M Kashif and M Singh *Appl. Numer. Math.* **207** 193 (2025). https://doi.org/10.1016/j.apnum.2024.08.019
[19] S Das, S K Mahato, A Mondal and E Kaslik *Nonlinear Dyn.* **111** 8821 (2023). https://doi.org/10.1007/s11071-023-08292-2
[20] J D Murray *Mathematical Biology I: An Introduction* (Cham: Springer) (2007)
[21] M J Ablowitz and A Zeppetella *Bull. Math. Biol.* **41** 835 (1979). https://doi.org/10.1007/BF02462380
[22] J Wang and Z Li *AIMS Math.* **10** 24997 (2025). https://doi.org/10.3934/math.20251107
[23] J H Choi, H Kim and R Sakthivel *J. Appl. Anal. Comput.* **7** 236 (2017). https://doi.org/10.11948/2017016
[24] M Areshi, A R Seadawy, A Ali, A F Alharbi and A F Aljohani *Fractal Fract.* **7** 128 (2023). https://doi.org/10.3390/fractalfract7020128
[25] B Tang *Complexity* **2021** 6402459 (2021). https://doi.org/10.1155/2021/6402459
[26] E V Nikolova *Springer Proc. Math. Stat.* **449** 267 (2024). https://doi.org/10.1007/978-3-031-53212-2_24
[27] M B A Mansour *Indian J. Phys.* **98** 4535 (2024). https://doi.org/10.1007/s12648-024-03190-8
[28] H Toumi, K Boudjema Djeffal, A Mezouaghi, R Darazirar and S Djilali *J. Acta Appl. Math.* **198** 3 (2025). https://doi.org/10.1007/s10440-025-00736-8
[29] S Djilali, R Darazirar and I Alraddadi *J. Appl. Math. Comput.* **71** 725 (2025). https://doi.org/10.1007/s12190-025-02474-4
[30] B Guenad, R Darazirar, S Djilali and I Alraddadi *Nonlinear Dyn.* **113** 3673 (2025). https://doi.org/10.1007/s11071-024-09369-7
[31] S Bentout, S Djilali and S Kumar *Phys. A* **572** 125840 (2021). https://doi.org/10.1016/j.physa.2021.125840
[32] S Djilali *Math. Methods Appl. Sci.* **43** 2233 (2020). https://doi.org/10.1002/mma.6036
[33] Z Wang, S Qiu, S Yu, B Wu and W Zhang *J. Comput. Math.* **41** 173 (2023). https://doi.org/10.4208/jcm.2107-m2020-0133
[34] Y Chen, Z Chen and Y Huang *J. Comput. Math.* **42** 355 (2024). https://doi.org/10.4208/jcm.2209-m2022-0129
[35] H Sakariya and S Kumar *Indian J. Phys.* **99** 5613 (2025). https://doi.org/10.1007/s12648-025-03740-8
[36] C Lee, Y Nam, M Bang, S Ham and J Kim *AIMS Math.* **9** 26671 (2024). https://doi.org/10.3934/math.20241297
[37] J Kim *Korean J. Math.* **33** 87 (2025). https://doi.org/10.11568/kjm.2025.33.2.87
[38] J Kim *Mathematics* **12** 3081 (2024). https://doi.org/10.3390/math12193081
[39] M Jornet and J J Nieto *Appl. Math. Lett.* **154** 109085 (2024). https://doi.org/10.1016/j.aml.2024.109085
[40] K A Lazopoulos and A K Lazopoulos *Prog. Fract. Differ. Appl.* **2** 67 (2016)
[41] J Wang, K Chen and J Kim *Phys. A* **665** 130500 (2025). https://doi.org/10.1016/j.physa.2025.130500
[42] S Kwak *J. KSIAM* **29** 2 171 (2025). https://doi.org/10.12941/jksiam.2025.29.171
[43] C Lee and J Kim *Phys. A* **680** 131052 (2025). https://doi.org/10.1016/j.physa.2025.131052
[44] H Zhang and J Yang *Commun. Nonlinear Sci. Numer. Simul.* **152** 109303 (2026). https://doi.org/10.1016/j.cnsns.2025.109303
[45] S Djilali *Chaos Solitons Fract.* **120** 139 (2019). https://doi.org/10.1016/j.chaos.2019.01.022